Eukaryotic Cell

Depletion of Mitochondrial Acyl Carrier Protein in Bloodstream-Form Trypanosoma brucei Causes a Kinetoplast Segregation Defect

April M. Clayton, Jennifer L. Guler, Megan L. Povelones, Eva Gluenz, Keith Gull, Terry K. Smith, Robert E. Jensen and Paul T. Englund

Eukaryotic Cell **2011, 10(3):286. DOI: 10.1128/EC.00290-10. Published Ahead of Print 14 January 2011.**

EUKARYOTIC CELL, Mar. 2011, p. 286–292 Vol. 10, No. 3
1535-9778/11/$12.00 doi:10.1128/EC.00290-10

Depletion of Mitochondrial Acyl Carrier Protein in Bloodstream-Form *Trypanosoma brucei* Causes a Kinetoplast Segregation Defect[▽]

April M. Clayton,[1]†‡ Jennifer L. Guler,[1]†§ Megan L. Povelones,[1]†¶ Eva Gluenz,[2] Keith Gull,[2] Terry K. Smith,[3] Robert E. Jensen,[4] and Paul T. Englund[1]*

Departments of Biological Chemistry[1] and Cell Biology,[4] Johns Hopkins University School of Medicine, Baltimore, Maryland; Sir William Dunn School of Pathology, University of Oxford, Oxford, United Kingdom[2]; and Centre for Biomolecular Sciences, The University of St. Andrews, Scotland, United Kingdom[3]

Received 16 November 2010/Accepted 5 January 2011

Like other eukaryotes, trypanosomes have an essential type II fatty acid synthase in their mitochondrion. We have investigated the function of this synthase in bloodstream-form parasites by studying the effect of a conditional knockout of acyl carrier protein (ACP), a key player in this fatty acid synthase pathway. We found that ACP depletion not only caused small changes in cellular phospholipids but also, surprisingly, caused changes in the kinetoplast. This structure, which contains the mitochondrial genome in the form of a giant network of several thousand interlocked DNA rings (kinetoplast DNA [kDNA]), became larger in some cells and smaller or absent in others. We observed the same pattern in isolated networks viewed by either fluorescence or electron microscopy. We found that the changes in kDNA size were not due to the disruption of replication but, instead, to a defect in segregation. kDNA segregation is mediated by the tripartite attachment complex (TAC), and we hypothesize that one of the TAC components, a differentiated region of the mitochondrial double membrane, has an altered phospholipid composition when ACP is depleted. We further speculate that this compositional change affects TAC function, and thus kDNA segregation.

Trypanosoma brucei, the African trypanosome, is a protozoan parasite that is transmitted by the tsetse fly vector. It causes human African trypanosomiasis (sleeping sickness) and related diseases in livestock. This parasite has been investigated extensively, not only because it causes disease but also because it has some remarkable biological properties.

One amazing feature, studied in our laboratory for many years, is the mitochondrial genome, known as kinetoplast DNA (kDNA) (reviewed in references 17 and 25). kDNA consists of several thousand minicircles (1 kb) and a few dozen maxicircles (23 kb), all concatenated into a giant planar network. Within the cell, the kDNA network is condensed into a disk-shaped structure known as the kinetoplast, which resides within the matrix of the trypanosome's single tubular mitochondrion. The kDNA disk is held in position by a transmembrane filament system known as the tripartite attachment complex (TAC). The three components of the TAC are a differentiated portion of the mitochondrial double membrane, unilateral filaments linking that membrane to the kDNA disk, and exclusion zone filaments connecting the membrane to the flagellar basal body that is in the cytoplasm (19, 23). This connection facilitates the segregation of newly replicated kDNA networks; as the basal bodies move apart, the daughter kinetoplasts are pulled into each of the progeny cells during cytokinesis (19, 23, 29).

In this paper, we report an unexpected link between kDNA and the mitochondrial fatty acid synthesis (FAS) system, which is another subject we have studied extensively in our laboratory. Trypanosomes (and related kinetoplastid parasites) assemble most of their fatty acids by using elongases in a mechanism fundamentally different from those of the type I and type II fatty acid synthases used by all other organisms (13, 14). (There are 4 enzymatic activities required for each cycle of addition of a two-carbon unit to a growing fatty acyl chain. In type II synthases, these activities are localized on separate polypeptide chains, and in type I synthases, they are localized on separate domains in a large polypeptide.) Elongases in other cell types extend preexisting long-chain fatty acids, but only the kinetoplastid parasites use this system for *de novo* FAS. Like other eukaryotes, trypanosomes also have a more conventional type II FAS system within the mitochondrion (1, 10, 26). Products of this pathway are octanoic acid (an 8-carbon precursor of lipoic acid which serves as a cofactor for several mitochondrial enzymes) and longer fatty acids (with the longest being palmitate, with 16 carbons) that are used in mitochondrial phospholipids. Acyl carrier protein (ACP), a key player in this pathway, forms a thioester linkage to the growing fatty acyl group and shuttles this molecule between the four enzymes responsible for sequential fatty acid chain growth.

A major objective of this project was to evaluate the significance of mitochondrial fatty acid synthesis in the two life cycle stages of *T. brucei* that are easily cultured in the laboratory. Based on RNA interference (RNAi) or conditional knockout

* Corresponding author. Mailing address: Department of Biological Chemistry, Johns Hopkins University School of Medicine, 725 N. Wolfe St., Baltimore, MD 21205. Phone: (410) 955-3790. Fax: (410) 955-7810. E-mail: penglund@jhmi.edu.

† A.M.C., J.L.G., and M.L.P. contributed equally to this work.

‡ Present address: Department of Molecular Microbiology and Immunology, Johns Hopkins University Bloomberg School of Public Health, Baltimore, MD.

§ Present address: Department of Chemistry, University of Washington, Seattle, WA.

¶ Present address: Division of Cell and Molecular Biology, Sir Alexander Fleming Building, Imperial College London, London, United Kingdom.

▽ Published ahead of print on 14 January 2011.

of ACP, we previously reported that mitochondrial FAS is essential for both insect-infecting (procyclic-form [PCF]) and mammal-infecting (bloodstream-form [BSF]) trypanosomes. While our previous studies on mitochondrial FAS focused mainly on PCFs (10, 26), we have now turned our attention to the more relevant (in terms of disease) BSF stage. As with our earlier studies on PCFs, we detected changes in cellular phospholipids following conditional knockout of ACP. Unexpectedly, we found that ACP depletion in BSF trypanosomes causes alterations in the kinetoplast size, and in some cells there is a complete loss of this structure. We and others have reported that RNAi-mediated kDNA loss is frequently associated with a defect in kDNA replication (for example, see references 5, 24, and 28). However, our studies presented in this paper indicate that ACP depletion has little effect on replication and that the kDNA effects are due to defective segregation of the progeny kDNA networks.

MATERIALS AND METHODS

Trypanosomes. Construction of the BSF *T. brucei* conditional knockout cell line for ACP was reported previously (26). Since deletion of both genomic ACP alleles was lethal, an ectopic copy of the ACP gene controlled by the tetracycline repressor was expressed during construction of the homozygous knockout. These cells were maintained at 37°C in 5% CO_2 and HMI-9 medium (11) containing 10% fetal bovine serum and 10% Serum Plus (JRH Biosciences). The antibiotic G418 (2.5 μg/ml) was used to maintain the T7 polymerase and *tet* repressor, while phleomycin (2.5 μg/ml) maintained the presence of the ectopic copy of ACP and tetracycline (Tet; 1 μg/ml) or doxycycline (1 μg/ml) allowed its expression.

ES-MS. ACP conditional knockout cells (~1×10^8 to 5×10^8) grown in the presence or absence of tetracycline for up to 6 days were harvested and extracted according to the method of Bligh and Dyer (3), dried under N_2, and stored at 4°C until analyzed by electrospray mass spectrometry (ES-MS) and ES-tandem MS (ES-MS/MS), as previously described (10).

Fluorescence microscopy. For staining of DNA in cells, 2 μg/ml of DAPI (4′,6-diamidino-2-phenylindole) was added to fixed cells, and the slides were mounted in Vectashield (Vector Laboratories). Following fixation, fluorescence *in situ* hybridization (FISH) was performed as described previously (7, 15). All imaging was done with a Zeiss Axioskop microscope equipped with a Retiga Exi charge-coupled-device (CCD) camera (QImaging Corp.).

Southern blotting. Total DNA isolation and Southern blotting were described previously (28). For analysis of free minicircle replication intermediates, total DNA was run directly in an agarose gel in the presence of ethidium bromide to resolve gapped and covalently closed species. To analyze total minicircle and maxicircle content, total DNA was digested with HindIII and XbaI prior to electrophoresis. kDNA species were detected on a Southern blot with ^{32}P-labeled probes for minicircles and maxicircles. The trypanosome hexose transporter (THT) gene was probed as a loading control.

DAPI staining and EM of isolated kDNA networks. kDNA networks were isolated as described previously (20), by centrifugation of cell lysates through a 20% sucrose cushion. For DAPI staining, 1 μl of isolated network solution was added to 19 μl of 1× phosphate-buffered saline (PBS). This solution was then spotted into one well of a 6-mm, 8-well slide coated with 0.01% poly-L-lysine. Networks were allowed to adhere to slides for 1 h, followed by washing with PBS. Finally, 2 μg/ml DAPI in PBS was added to the slide and incubated for 5 min. Slides were washed briefly with PBS and then mounted in Vectashield (Vector Laboratories) and examined by fluorescence microscopy as described above. IPLab software (Scanalytics, Inc.) was used for imaging and for network surface area measurements (6). For electron microscopy (EM), isolated networks were spread on nitrocellulose-coated grids by the formamide method (21). The grids were then rotary shadowed with Pt-Pd, using a Denton vacuum evaporator (DV502-A). DNA was imaged with a Phillips (CM-120) transmission electron microscope operating at 80 kV, recorded with an Orius SC 1004 2k×2× CCD camera, and digitized with a Gatan v. 3.11.0 digital micrograph. Brightness and contrast of some EM and fluorescence images were adjusted uniformly by using Adobe Photoshop on a Macintosh computer.

Thin-section EM. ACP knockout cells were grown in the presence of 1 μg/ml doxycycline (with similar effects to those with tetracycline) or in the absence of doxycycline for 3 days. Cells were fixed in 2.5% glutaraldehyde, postfixed in osmium tetroxide, and embedded in Epon (2). Thin sections were examined on an FEI Tecnai 12 transmission electron microscope.

RESULTS

Depletion of ACP in BSFs alters phospholipid content. Our previous study on PCF trypanosomes revealed that RNAi knockdown of ACP, and thus the mitochondrial FAS pathway, decreased phosphatidylinositol (PI) and phosphatidylethanolamine (PE) levels. This observation established the importance of mitochondrial FAS in the maintenance of phospholipid content (10). To investigate whether mitochondrial FAS has the same role in BSFs, we analyzed phospholipid content in cells with a conditional knockout of ACP (26). In these cells, we replaced both ACP alleles with drug resistance genes, but since ACP is essential for growth, we also introduced an ectopic copy of the ACP gene whose expression depended on the addition of Tet or doxycycline to the culture medium. As in our experiments with PCFs (10), we then used ES-MS to compare the phospholipid content of whole-cell extracts of BSF cells expressing ACP (measured at day 0, prior to removal of Tet) with that of similar extracts of BSF cells grown in the absence of Tet for 4 or 6 days. To search for major changes in levels of various phospholipids, we first conducted survey scans in negative-ion mode, for detection of PI, PE, phosphatidylserine (PS), phosphatidylglycerol (PG), and phosphatidic acid (PA) (Fig. 1A), and in positive-ion mode, mainly for detection of phosphatidylcholine (PC) and sphingomyelin (SM) (Fig. 1B). The molecular species for the above phospholipid classes have previously been characterized for *T. brucei* BSFs (22).

From the negative-ion survey scan (Fig. 1A), we observed that the ratios of the major PS (772 *m/z*; alkyl-$C_{18:0}$ and $C_{18:2}$) and PI (912 *m/z*; $C_{18:0}$ and $C_{22:5}$) species remained relatively constant, while the major PE peak (726 *m/z*; alkyl-$C_{18:1}$ and $C_{18:2}$) decreased by day 4 of ACP depletion (Fig. 1A, day 0; these 3 phospholipids are marked with asterisks). This observation was supported by further investigation of the collision-induced daughter ion characteristic of PE phospholipids (parents of 196 *m/z*) by ES-MS/MS, where a decrease in the major plasmenyl-PE was observed by day 6 (Fig. 2A, 726 *m/z*). The ion at 659 *m/z*, previously identified as ethanolamine-phosphorylceramide (27), changed little; its apparent increase at day 6 was due to the significant decrease in PE (726 *m/z*). This decrease in PE upon ACP loss paralleled relative increases in the phospholipids PA (737 *m/z*; alkyl-$C_{18:0}$ and $C_{22:4}$) and PG (805 *m/z* [$C_{18:0}$ and $C_{20:0}$], 821 *m/z* [$C_{18:0}$ and $C_{22:5}$], and 869 *m/z* [$C_{22:4}$ and $C_{22:5}$]) (Fig. 1A, day 6 [marked with asterisks]). Further investigation of the PS species by collision-induced fragmentation (neutral loss of 87 *m/z*) showed only a slight decrease in diacyl-PS, while PI species (parents of 241 *m/z*) showed insignificant fluctuations in level after ACP depletion (data not shown).

We detected minor changes in the positive-ion survey scan at day 6 compared with day 0 (Fig. 1B). We further investigated these potential differences by collision-induced parent ion scanning of 184 *m/z*, which is characteristic of PC and SM phospholipids (Fig. 2B). Changes in the PC and SM phospholipid content after 4 days of ACP depletion became more severe by day 6. These differences included relative increases in

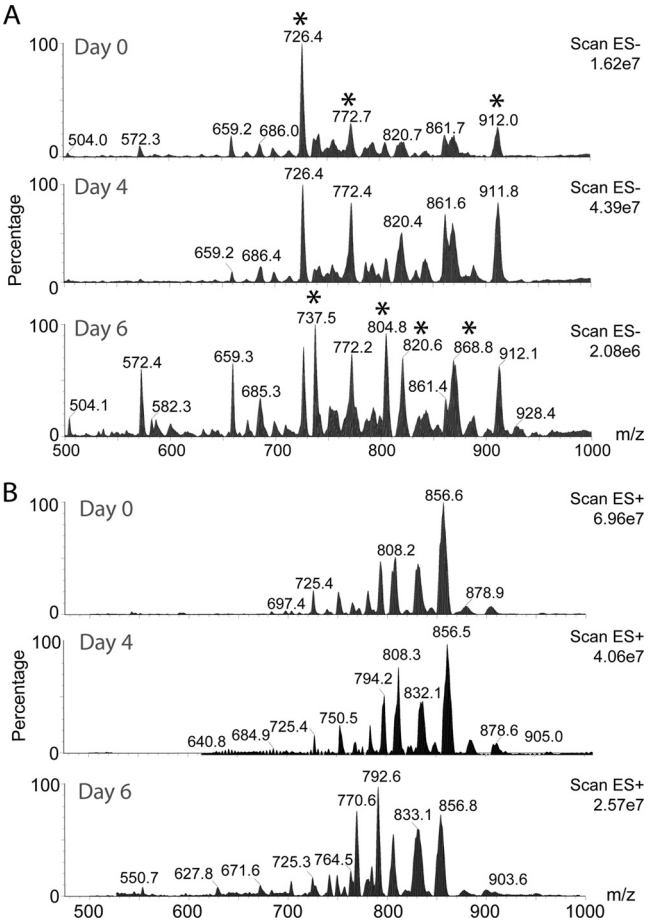

FIG. 1. Effect of ACP depletion on phospholipid content of BSF trypanosomes. Negative-ion (A) and positive-ion (B) ES-MS survey scans (500 to 1,000 *m/z*) of total lipid extracts from ACP-depleted BSF cells at days 0, 4, and 6. The following phospholipids discussed in the text are marked with asterisks: day 0, PE (726 *m/z*), PS (772 *m/z*), and PI (912 *m/z*); and day 6, PA (737 *m/z*) and PG (805, 821, and 869 *m/z*). The total ion count is shown in the top right corner of each spectrum in this and the following figure and is relative between spectra.

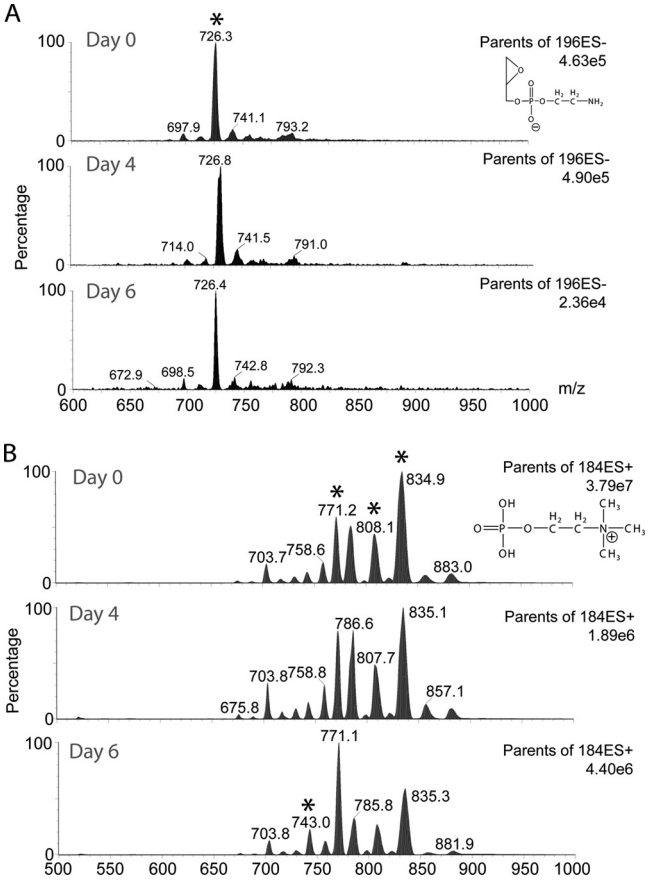

FIG. 2. Effect of ACP depletion on PE and PC levels. Lipids were extracted from ACP-depleted BSF cells at days 0, 4, and 6, as indicated, and analyzed by ES-MS/MS for PE phospholipids (parent-ion scanning of the 196 *m/z* fragment [see structure]) (A) and PC and SM phospholipids (parent-ion scanning of the 184 *m/z* fragment [see structure]) (B) as described in Materials and Methods. The following phospholipids discussed in the text are marked with asterisks: PE (726 *m/z*) (A), plasmenyl-PC (743 and 771 *m/z*) (B), and diacyl-PC (808 and 835 *m/z*) (B).

plasmenyl-PC species at 743 *m/z* ($C_{34:1}$) and 771 *m/z* ($C_{36:1}$ and alkyl-$C_{18:0/18:2}$), with corresponding decreases in diacyl-PC species at 807 *m/z* ($C_{18:0/20:4}$ and $C_{16:0/22:4}$) and 835 *m/z* ($C_{18:0}$ and $C_{22:5}$) (Fig. 2B, day 6 [marked with asterisks]). Thus, we concluded that ACP depletion alters the phospholipid content of BSF trypanosomes by decreasing PE, increasing PA and PG, and shifting to more plasmenyl-PC at the expense of diacyl-PC.

kDNA size and replication following ACP depletion. Again using the ACP conditional knockout, we found that BSF cells had significant changes in kinetoplast size that began prior to growth arrest (Fig. 3A and B). This observation was unexpected, as we had detected no effect on kDNA following RNAi-mediated knockdown of ACP in PCF trypanosomes (10, 26). Using fluorescence analysis of DAPI-stained cells, we evaluated the kinetics of kinetoplast size change during the days following Tet removal (Fig. 3B shows DAPI-stained examples of kinetoplasts of various sizes). After 4 days, we observed that approximately 25% of cells had no kinetoplast, 6% had kinetoplasts that were smaller than normal, and 19% had kDNA that appeared larger than normal (Fig. 3B).

We next used Southern blot analysis of minicircles and maxicircles as an alternative approach for evaluating kDNA levels. Surprisingly, we observed no significant change in level of either minicircles or maxicircles following Tet removal (Fig. 3C). Since these Southern blots reflect the kDNA content of the entire population after ACP removal, these data suggest that the DAPI-stained cells in Fig. 3B that appear to have less kDNA (small kinetoplasts or none at all) and those with more kDNA (large kinetoplasts) cancel each other out, leaving little, if any, net change in the level of minicircles or maxicircles (Fig. 3C).

Since kDNA loss could be due to a replication defect, we then looked for changes in free minicircle replication intermediates. kDNA replication (reviewed in references 17 and 25) involves release of monomeric covalently closed minicircles from the network, most likely by a topoisomerase II, followed by replication of the free minicircles to produce gapped progeny. These reattach to the network in another topoisomerase

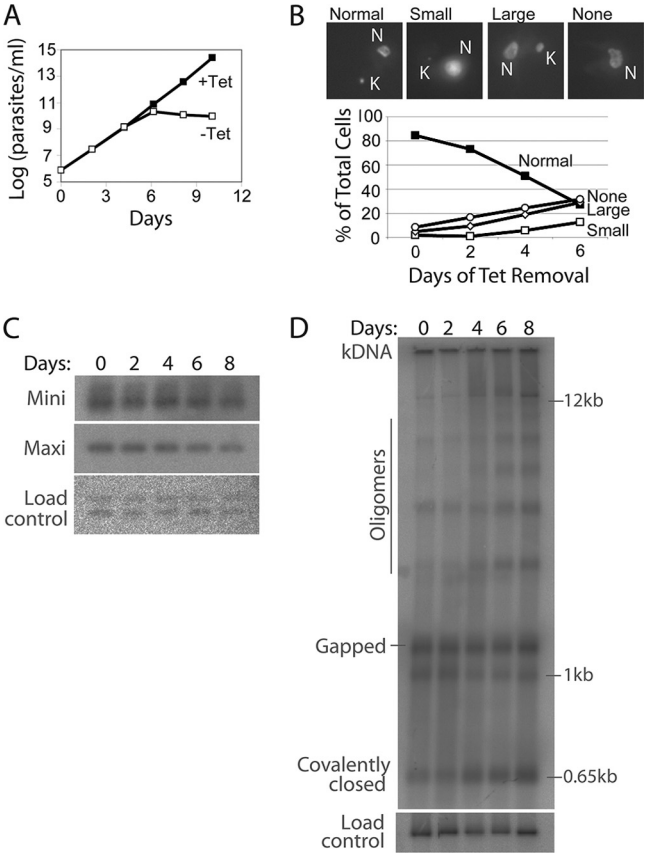

FIG. 3. Other effects of ACP depletion on BSF trypanosomes. (A) Growth curve showing the effect of ACP conditional knockout. ACP was expressed in cells cultured with 1 μg/ml of tetracycline in the medium (+tet) and was depleted when tetracycline was removed at day 0 (−tet). The number of parasites per milliliter was calculated by multiplying the cell density and the dilution factor. We demonstrated previously by Western blotting that ACP protein is almost nondetectable within 1 day after tetracycline removal (26). (B) Evaluation of kinetoplast size by visual inspection of DAPI-stained cells following tetracycline removal. Following fixation and staining, approximately 130 cells were scored for kinetoplast size at each time point. Images of DAPI-stained cells show examples of each kinetoplast size. K, kinetoplast; N, nucleus. (C) Southern blot analysis of total minicircle and maxicircle levels during 8 days of ACP depletion. Total DNA (1.5×10^7 to 2×10^7 cells/sample) was digested with HindIII and XbaI and fractionated by agarose gel electrophoresis, and a Southern blot was probed for minicircles (mini), maxicircles (maxi), or the trypanosome hexose transporter (load control). The figure shows a phosphorimaging scan of the Southern blot. The maxicircle probe recognized only a 1.4-kb fragment, and the minicircle probe recognized multiple fragments derived from the heterogeneous minicircle population. Only the 1-kb minicircle fragment is shown; other fragments deriving from the heterogeneous population behaved similarly. (D) Southern blot analysis of free minicircle replication intermediates during 8 days of ACP depletion. Undigested total DNA was fractionated by agarose gel electrophoresis with ethidium bromide and then probed for minicircles or the trypanosome hexose transporter (load control). Intact kDNA networks remain in the wells (kDNA). Predominant minicircle species were covalently closed (replication precursors) and gapped (replication products) species. The 1-kb fragment represents linearized minicircles. Minicircle oligomers are indicated.

reaction. These closed and gapped free minicircles are easily separated by agarose gel electrophoresis in the presence of ethidium bromide. Autoradiography of a Southern blot showed that in the days following tetracycline removal, there were no major changes in these free minicircle species, except for a slight increase in oligomeric forms (designated "oligomers" in Fig. 3D). These experiments provided strong evidence that ACP depletion had little effect on minicircle replication.

Changes in kDNA structure following ACP depletion. To examine more closely the structure of kDNA networks following ACP depletion, we isolated networks from cells before (day 0) and after (days 2 and 4) ACP depletion (by Tet removal), stained them with DAPI, examined them by fluorescence microscopy, and measured the surface area of about 130 networks at each time point (Fig. 4A). The size distributions of networks isolated from cells expressing ACP (day 0) and from those after ACP depletion for 2 days centered around unit-size networks (~5 μm^2). However, after 4 days of ACP depletion, the distribution of network surface areas became much more heterogeneous, with more networks being smaller or larger than unit size (Fig. 4A). These measurements were consistent with our in-cell observations and provided support for the hypothesis that most ACP-depleted cells contained networks that were small, normal, or large. The larger networks rarely exceeded a doubled size, which is the size of a network after replication and prior to segregation.

We also considered the possibility that network size changes reflected alterations in network topology. Minicircles in the kDNA network are each concatenated to several neighboring minicircles, and the number of neighbors varies according to the stage of kDNA replication (4). The number of interlocks per minicircle determines the minicircle density and therefore can affect network size. For example, if the minicircle density decreases due to a reduction in the average number of neighbors of each minicircle, the network expands in terms of surface area (4). Similarly, an increase in minicircle density would shrink the network surface area. Finally, if networks develop holes, as occurs when monomeric minicircles are released for replication, they also enlarge significantly (16); these holes are observed following RNAi of the mitochondrial topoisomerase II. To evaluate these possibilities, we employed EM (Fig. 4B) to examine isolated networks following ACP depletion. These experiments revealed neither holes nor obvious changes in minicircle density. However, as shown by the examples in Fig. 4B, we did observe considerable variation in network size at day 4. Compared to the normally sized network at day 0 (upper left), day 4 networks were either normal (lower left), large (upper right), or small (lower right), consistent with the histograms in Fig. 4A. Regardless of their variation in size, most networks at day 4 appeared to have a relatively normal shape.

kDNA segregation following ACP depletion. kDNA replication produces a double-size network that splits into two equal-size progeny, which then segregate into daughter cells during cytokinesis. The fact that some ACP-depleted cells had large kDNA networks while others had small kDNA networks or none at all raised the possibility of a defect in kDNA segregation. A complete block in segregation would produce a cell with a double-size network and a sister cell with none at all, consistent with our observations. In another, less severe type of segregation defect, the double-size product of replication divides asymmetrically, leading to one progeny network that is larger than normal and one that is smaller, again consistent with our observations. To explore the possibility of asymmetric segregation, we DAPI-stained cells following depletion of

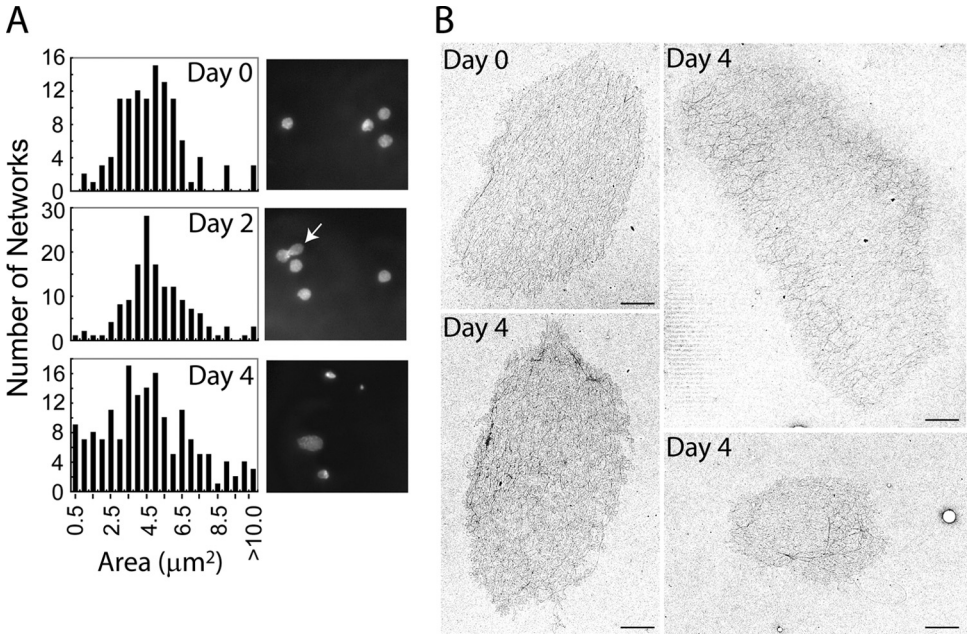

FIG. 4. Effects of ACP depletion on kDNA size and topology. (A) Surface areas of isolated kDNA networks following ACP depletion. Networks were stained with DAPI and visualized by fluorescence microscopy (right panels), and their surface areas were measured by IPLab software (29). At each time point, 100 to 130 networks were measured. In the histograms, unit-size and double-size networks are not well resolved. Note that the *y* axis differs for each histogram. The arrow in the day 2 image indicates a dumbbell-shaped dividing kDNA network. (B) EM of isolated kDNA networks. The top left panel shows a representative day 0 (+Tet) network, while the other panels show examples of large, small, and normally sized networks isolated 4 days after tetracycline removal. Bars, 1 μm.

ACP. Fluorescence microscopy revealed that by day 6, about 18% of all cells had asymmetrically dividing kinetoplasts (Fig. 5A). We also detected cells with small DAPI-staining structures that appeared to be positioned distant from the kinetoplast but presumably within the mitochondrial matrix (Fig. 5B). Such structures, known as ancillary kDNA, have been observed previously in wild-type trypanosomatids (mainly *Trypanosoma cruzi*) (18) and in RNAi cell lines (e.g., following knockdown of DNA polymerase IC [12]). These are thought to be small network fragments in abnormal positions within the mitochondrial matrix. Examination of cells 4 days after ACP depletion revealed that 13% (15/116 cells) contained ancillary kDNA (Fig. 5B). To determine if these small DAPI-stained structures were actually ancillary kDNA and not, for example, nuclear DNA fragments, we used FISH with minicircle and maxicircle probes. Ancillary kDNA was detectable with the minicircle probe, proving that these structures were in fact small fragments of kDNA (Fig. 5B). We could not detect maxicircles in ancillary kDNA, either because they were not present or because their level was too low to detect. Also, if they were covalently closed, they would be nondenaturable and therefore unable to hybridize with the probe. This result suggests that ACP loss may promote network fragmentation and that the fragments may disconnect from the TAC.

Mitochondrial structure following ACP depletion. Electron microscopy of PCFs following ACP depletion revealed mitochondrial enlargement and abnormal ultrastructural features, such as membranous bodies thought to be disrupted cristae (10). We performed thin-section EM on ACP-depleted BSF trypanosomes 3 days after Tet removal to assess whether structural abnormalities of the mitochondrion could help to explain the segregation defect in this life cycle stage. Control cells prior to tetracycline removal displayed unit-size kDNA networks surrounded by a tightly fitting mitochondrial membrane (Fig. 5C, day 0 [K]). In day 3 cells, basal bodies appeared properly aligned with the kDNA disk (Fig. 5C, black arrowheads), and flagellar pockets were properly formed (white arrowheads). We observed large and possibly abnormally dividing kinetoplasts (K) after 3 days of ACP depletion. Overall, the mitochondrial structure appeared normal in size and density, but membranous bodies (white arrows) were present within some ACP-depleted BSF mitochondria.

DISCUSSION

Our initial objective in this study was to evaluate the effects of ACP depletion on BSF trypanosomes. This in turn might reveal some of the functions of mitochondrial fatty acid synthesis, an essential biochemical pathway in this life cycle stage. As with PCFs (10), our lipid analyses with BSFs (Fig. 1 and 2) showed that depletion of ACP and subsequent inactivation of mitochondrial FAS caused alterations in the levels of some cellular phospholipids (Fig. 1 and 2). Although the decreases in BSF PE and diacyl-PC were small (Fig. 2A and B), these alterations occurred around the same time as the disturbance in kDNA segregation (see below). Unfortunately, we were unable to isolate mitochondria from ACP-depleted BSF trypanosomes because of their fragile nature (possibly due to their altered phospholipid content), and therefore we could not assess phospholipid levels in this organelle (as we did following RNAi knockdown of ACP in PCFs [10]). We assume that the phospholipids produced by mitochondrial FAS are

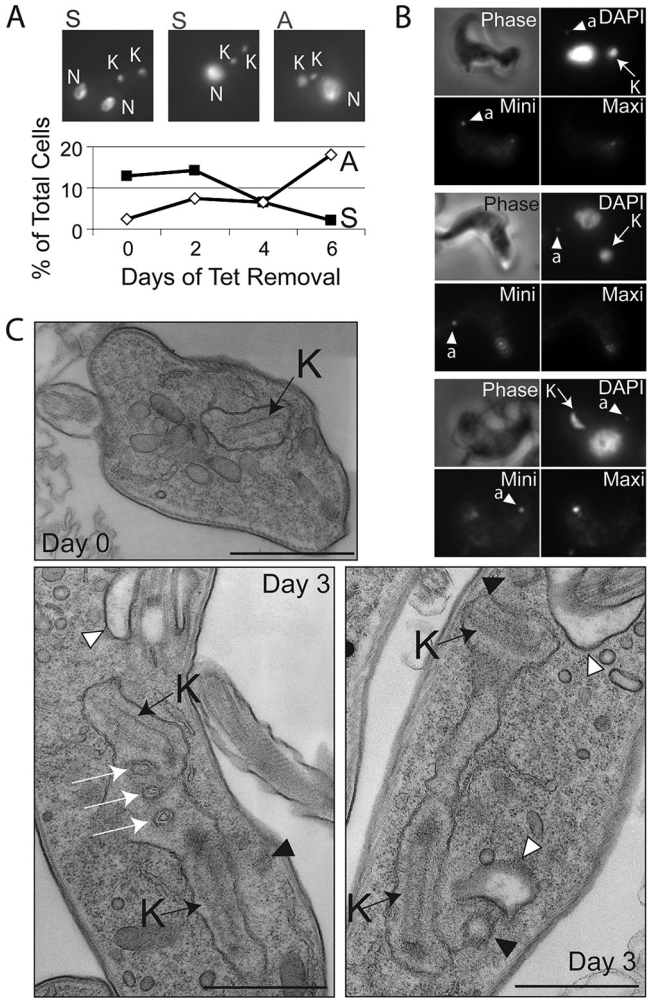

FIG. 5. Effects of ACP depletion on kDNA segregation and cell structure. (A) Quantitation of asymmetrical kinetoplast division following ACP depletion. Cells were fixed, stained with DAPI, visualized by fluorescence microscopy, and scored for symmetrical (S) and asymmetrical (A) division of kinetoplasts. The images are DAPI-stained examples of each type. K, kDNA; N, nucleus. (B) DAPI and FISH staining of three cells containing ancillary kDNA (a; arrowhead) anterior to the nucleus and of a kinetoplast in its normal position in the posterior of the cell (K; arrow). The minicircle FISH probe does not detect covalently closed minicircles (which are nondenaturable), explaining why the FISH staining of the kDNA networks does not match the DAPI signal. (C) Thin-section electron micrographs of BSF trypanosomes prior to removal of doxycycline from the medium (day 0) and after its removal (day 3). The black arrow (K) points to the kDNA nucleoid, which in cross-section appears as a bar-shaped structure. White arrowheads indicate the flagellar pocket, black arrowheads indicate basal bodies and probasal bodies, and white arrows indicate membranous bodies within the mitochondrion in ACP-depleted BSF trypanosomes. Bars, 800 nm.

destined for the mitochondrial membranes, and therefore the small changes detected in whole-cell extracts may represent a much larger local change in the mitochondrial phospholipids.

The striking effect of ACP depletion in BSFs concerned kinetoplast size, with some cells developing large kinetoplasts, some developing small ones, and others losing this structure completely. We found that minicircle replication proceeds fairly normally in BSFs following conditional knockout of ACP (Fig. 3D), and therefore a defect in this process is unlikely a cause of the phenotype. Instead, our experiments indicated that the kinetoplast size change is due to a defect in network segregation. Normally, the double-size network that is the product of replication undergoes scission in the center to form two networks that are equal in size to each other and to the parent. If segregation is defective, the double-size network can divide asymmetrically, yielding one daughter which is larger than normal and another which is correspondingly smaller. In the extreme case, the double-size network may not divide at all: at cell division, one cell inherits the whole double-size network and the other cell receives no kDNA.

Prior to this study, our understanding of defective kDNA segregation was based largely on our previous investigations of PCF cells depleted of p166, the first protein component of the TAC to be discovered (29). Now we have found that the major difference between the segregation defects following p166 RNAi and the conditional knockout of ACP is that p166 loss causes a more profound segregation defect than does ACP loss. For example, in p166 RNAi PCF cells, the large kinetoplasts are often larger than the nucleus; in addition, isolated networks are occasionally 10 times larger in area than a wild-type network. This massive enlargement requires several generations, during which the already large kinetoplast grows progressively larger. In contrast, in ACP-depleted cells, networks rarely exceed a doubled size, suggesting that the undivided double-size kinetoplasts cannot undergo further replication. There are several possible explanations for why depletion of p166 in PCFs or ACP in BFSs leads to such different effects on kDNA segregation. One is related to cell cycle control. BSF cells could have a cell cycle checkpoint that prevents overreplication of kDNA in the absence of segregation, and PCF cells could lack this checkpoint; thus, the difference would be due to life cycle stage, which could be checked by studying the effects of p166 depletion in BSF parasites. Another possible explanation is discussed below.

How can a change in phospholipid content resulting from ACP depletion affect kDNA segregation? One exciting possibility is that the defect in fatty acid synthesis affects the membrane component of the TAC. Although nothing is known about its phospholipid composition, this specialized double membrane is resistant to detergent extraction, devoid of cristae, and more electron dense than contiguous mitochondrial membranes. The TAC double membrane anchors the exclusion zone filaments that connect to the basal body in the cytoplasm and also the unilateral filaments that link to the kinetoplast in the mitochondrial matrix (9, 19, 23). Altering this membrane's composition could affect TAC structure, thus decreasing the fidelity of kDNA segregation.

If our speculation that the effect of ACP depletion on kDNA segregation is due to changes in the TAC's membrane component is correct, it could explain why the depletion of ACP and p166 has such different effects. In one case, there is modification of a membrane, and in the other case, there is loss of a protein. Altering the TAC in these two different ways could have very different effects on segregation. It might also explain why ancillary kDNA is produced in one case but not the other.

It was surprising that a kDNA segregation defect was seen after ACP depletion in BSFs but not in PCFs. Although it is possible that the differences are technical (e.g., we used differ-

ent methods to deplete ACP in BSFs and PCFs), we think the answer more likely lies in the different metabolic pathways found in the two life cycle stages. PCF trypanosomes rely on a conventional mitochondrial respiratory chain that is absent in BSFs. Respiratory activity is disrupted during RNAi knockdown of ACP, presumably because of the requirement of certain mitochondrially produced phospholipids for assembly of PCF respiratory complexes (10). Thus, the effects of ACP loss on TAC and kDNA may be the same in PCFs and BSFs, but we believe that the PCF cells die of a respiration defect prior to emergence of the kDNA segregation phenotype.

A reduction in PCF sphingolipid synthesis caused by RNAi knockdown of serine palmitoyltransferase also impaired kDNA segregation (8), and this defect could also be due to abnormalities in the mitochondrial membrane. If the sphingolipid deficiency does not affect respiration, then these PCF cells might survive long enough to demonstrate effects on kDNA. However, this deficiency in sphingolipid synthesis also affects cytokinesis; therefore, it is unclear if delayed kinetoplast segregation is a primary or secondary effect of impaired cell cycle progression (8).

A long-term goal in our laboratory is to understand the structure of the TAC and how it mediates kDNA segregation. Cell lines undergoing RNAi for various protein components of the TAC filaments will be valuable in this regard. Along these lines, if our speculation is correct, then the ACP conditional knockout cell line could be used to alter the composition of the membrane component of the TAC.

ACKNOWLEDGMENTS

We thank members of our lab for helpful discussions and Gokben Yildirir for assistance. Mike Shaw helped with thin-section EM, and Mike Delannoy helped with EM of isolated networks.

P.T.E. was supported by NIH grants AI058613 and AI21334, R.E.J. was supported by NIH grant GM54021, K.G. was supported by a Wellcome Trust principal fellowship and a Wellcome Trust program grant, and T.K.S. was supported by a Wellcome Trust senior research fellowship (067441) and Wellcome Trust project grant 086658.

REFERENCES

1. **Autio, K. J., J. L. Guler, A. J. Kastaniotis, P. T. Englund, and J. K. Hiltunen.** 2008. The 3-hydroxyacyl-ACP dehydratase of mitochondrial fatty acid synthesis in *Trypanosoma brucei*. FEBS Lett. **582:**729–733.
2. **Baines, A., and K. Gull.** 2008. WCB is a C2 domain protein defining the plasma membrane-sub-pellicular microtubule corset of kinetoplastid parasites. Protist **159:**115–125.
3. **Bligh, E. G., and W. J. Dyer.** 1959. A rapid method of total lipid extraction and purification. Can. J. Biochem. Physiol. **37:**911–917.
4. **Chen, J., P. T. Englund, and N. R. Cozzarelli.** 1995. Changes in network topology during the replication of kinetoplast DNA. EMBO J. **14:**6339–6347.
5. **Downey, N., J. C. Hines, K. M. Sinha, and D. S. Ray.** 2005. Mitochondrial DNA ligases of *Trypanosoma brucei*. Eukaryot. Cell **4:**765–774.
6. **Drew, M. E., and P. T. Englund.** 2001. Intramitochondrial location and dynamics of *Crithidia fasciculata* kinetoplast minicircle replication intermediates. J. Cell Biol. **153:**735–744.
7. **Ferguson, M. L., A. F. Torri, D. Perez-Morga, D. C. Ward, and P. T. Englund.** 1994. Kinetoplast DNA replication: mechanistic differences between *Trypanosoma brucei* and *Crithidia fasciculata*. J. Cell Biol. **126:**631–639.
8. **Fridberg, A., et al.** 2008. Sphingolipid synthesis is necessary for kinetoplast segregation and cytokinesis in *Trypanosoma brucei*. J. Cell Sci. **121:**522–535.
9. **Gluenz, E., M. K. Shaw, and K. Gull.** 2007. Structural asymmetry and discrete nucleic acid subdomains in the *Trypanosoma brucei* kinetoplast. Mol. Microbiol. **64:**1529–1539.
10. **Guler, J. L., E. Kriegova, T. K. Smith, J. Lukes, and P. T. Englund.** 2008. Mitochondrial fatty acid synthesis is required for normal mitochondrial morphology and function in *Trypanosoma brucei*. Mol. Microbiol. **67:**1125–1142.
11. **Hirumi, H., and K. Hirumi.** 1989. Continuous cultivation of *Trypanosoma brucei* blood stream forms in a medium containing a low concentration of serum protein without feeder cell layers. J. Parasitol. **75:**985–989.
12. **Klingbeil, M. M., S. A. Motyka, and P. T. Englund.** 2002. Multiple mitochondrial DNA polymerases in *Trypanosoma brucei*. Mol. Cell **10:**175–186.
13. **Lee, S. H., J. L. Stephens, and P. T. Englund.** 2007. A fatty-acid synthesis mechanism specialized for parasitism. Nat. Rev. Microbiol. **5:**287–297.
14. **Lee, S. H., J. L. Stephens, K. S. Paul, and P. T. Englund.** 2006. Fatty acid synthesis by elongases in trypanosomes. Cell **126:**691–699.
15. **Li, Z., M. E. Lindsay, S. A. Motyka, P. T. Englund, and C. C. Wang.** 2008. Identification of a bacterial-like HslVU protease in the mitochondria of *Trypanosoma brucei* and its role in mitochondrial DNA replication. PLoS Pathog. **4:**e1000048.
16. **Lindsay, M. E., E. Gluenz, K. Gull, and P. T. Englund.** 2008. A new function of *Trypanosoma brucei* mitochondrial topoisomerase II is to maintain kinetoplast DNA network topology. Mol. Microbiol. **70:**1465–1476.
17. **Liu, B., Y. Liu, S. A. Motyka, E. E. C. Agbo, and P. T. Englund.** 2005. Fellowship of the rings: the replication of kinetoplast DNA. Trends Parasitol. **21:**363–369.
18. **Miyahira, Y., and J. A. Dvorak.** 1994. Kinetoplastidae display naturally occurring ancillary DNA-containing structures. Mol. Biochem. Parasitol. **65:**339–349.
19. **Ogbadoyi, E. O., D. R. Robinson, and K. Gull.** 2003. A high-order transmembrane structural linkage is responsible for mitochondrial genome positioning and segregation by flagellar basal bodies in trypanosomes. Mol. Biol. Cell **14:**1769–1779.
20. **Pérez-Morga, D., and P. T. Englund.** 1993. The attachment of minicircles to kinetoplast DNA networks during replication. Cell **74:**703–711.
21. **Pérez-Morga, D. L., and P. T. Englund.** 1993. Microtechnique for electron microscopy of DNA. Nucleic Acids Res. **21:**1328–1329.
22. **Richmond, G. S., et al.** 2010. Lipidomic analysis of bloodstream and procyclic form *Trypanosoma brucei*. Parasitology **137:**1357–1392.
23. **Robinson, D. R., and K. Gull.** 1991. Basal body movements as a mechanism for mitochondrial genome segregation in the trypanosome cell cycle. Nature **352:**731–733.
24. **Scocca, J. R., and T. A. Shapiro.** 2008. A mitochondrial topoisomerase IA essential for late theta structure resolution in African trypanosomes. Mol. Microbiol. **67:**820–829.
25. **Shlomai, J.** 2004. The structure and replication of kinetoplast DNA. Curr. Mol. Med. **4:**623–647.
26. **Stephens, J. L., S. H. Lee, K. S. Paul, and P. T. Englund.** 2007. Mitochondrial fatty acid synthesis in *Trypanosoma brucei*. J. Biol. Chem. **282:**4427–4436.
27. **Sutterwala, S. S., et al.** 2008. Developmentally regulated sphingolipid synthesis in African trypanosomes. Mol. Microbiol. **70:**281–296.
28. **Wang, Z., and P. T. Englund.** 2001. RNA interference of a trypanosome topoisomerase II causes progressive loss of mitochondrial DNA. EMBO J. **20:**4674–4683.
29. **Zhao, Z., M. E. Lindsay, A. Roy Chowdhury, D. R. Robinson, and P. T. Englund.** 2008. p166, a link between the trypanosome mitochondrial DNA and flagellum, mediates genome segregation. EMBO J. **27:**143–154.